AIP Advances

Strain effect in epitaxial VO_2 thin films grown on sapphire substrates using SnO_2 buffer layers

Cite as: AIP Advances 7, 105116 (2017); https://doi.org/10.1063/1.5004125
Submitted: 11 September 2017 . Accepted: 18 October 2017 . Published Online: 26 October 2017

Heungsoo Kim, Nicholas S. Bingham, Nicholas A. Charipar, and Alberto Piqué

COLLECTIONS

Paper published as part of the special topic on Chemical Physics, Energy, Fluids and Plasmas, Materials Science and Mathematical Physics

View Online

Export Citation

CrossMark

ARTICLES YOU MAY BE INTERESTED IN

Metal-insulator transition of VO_2 thin films grown on TiO_2 (001) and (110) substrates
Applied Physics Letters **80**, 583 (2002); https://doi.org/10.1063/1.1446215

Structural, electrical, and terahertz transmission properties of VO_2 thin films grown on c-, r-, and m-plane sapphire substrates
Journal of Applied Physics **111**, 053533 (2012); https://doi.org/10.1063/1.3692391

Selective growth of single phase VO_2(A, B, and M) polymorph thin films
APL Materials **3**, 026101 (2015); https://doi.org/10.1063/1.4906880

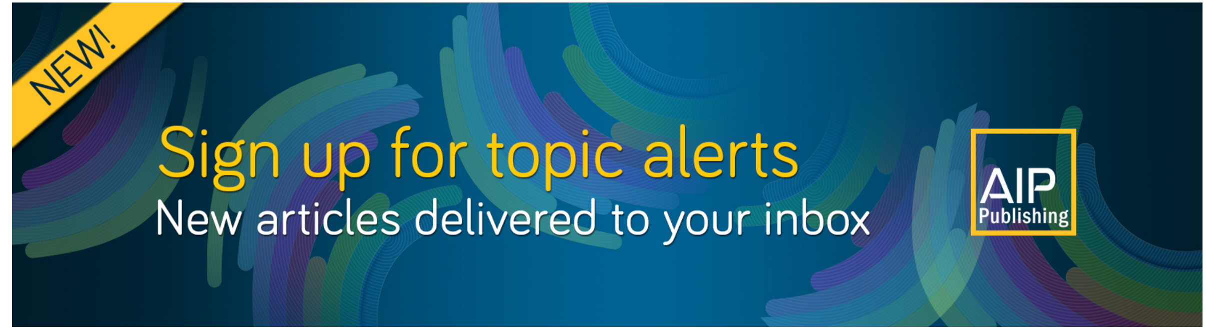

© 2017 Author(s).

AIP ADVANCES 7, 105116 (2017)

Strain effect in epitaxial VO_2 thin films grown on sapphire substrates using SnO_2 buffer layers

Heungsoo Kim,[1,a] Nicholas S. Bingham,[2] Nicholas A. Charipar,[1] and Alberto Piqué[1]
[1]*Naval Research Laboratory, Washington, DC 20375, USA*
[2]*National Research Council Fellow at the Naval Research Laboratory, Washington, DC 20375, USA*

(Received 11 September 2017; accepted 18 October 2017; published online 26 October 2017)

Epitaxial VO_2/SnO_2 thin film heterostructures were deposited on m-cut sapphire substrates via pulsed laser deposition. By adjusting SnO_2 (150 nm) growth conditions, we are able to control the interfacial strain between the VO_2 film and SnO_2 buffer layer such that the semiconductor-to-metal transition temperature (T_C) of VO_2 films can be tuned without diminishing the magnitude of the transition. It is shown that in-plane tensile strain and out-of-plane compressive strain of the VO_2 film leads to a decrease of Tc. Interestingly, VO_2 films on SnO_2 buffer layers exhibit a structural phase transition from tetragonal-like VO_2 to tetragonal-VO_2 during the semiconductor-to-metal transition. These results suggest that the strain generated by SnO_2 buffer provides an effective way for tuning the T_C of VO_2 films. © *2017 Author(s). All article content, except where otherwise noted, is licensed under a Creative Commons Attribution (CC BY) license (http://creativecommons.org/licenses/by/4.0/).* https://doi.org/10.1063/1.5004125

I. INTRODUCTION

VO_2 has gained considerable interest due to its first-order phase transition between a low-temperature monoclinic phase (semiconducting state) and a high-temperature tetragonal phase (metallic state) at a transition temperature (T_C) ~ 68 °C.[1] This semiconductor-to-metal transition (SMT) can be induced thermally,[2] electrically,[3] or optically,[4] and it can occur at ultrafast timescales (~100fs).[5] Upon transitioning to the metallic phase, the electrical resistance decreases by four orders of magnitude and the optical transmittance in the near infrared decreases by as much as 60 %. Because of these unique properties, VO_2 has been exploited in various devices such as Mott field effect transistors,[6,7] ultrafast switches,[8,9] memristors,[10] plasmonic metamaterials,[11–13] and smart windows.[14]

In order to use VO_2 thin films as a technologically relevant material, it is necessary for its T_C to be tunable to fulfill specific working environments in various devices.[15,16] Many efforts have been focused on tuning the T_C of VO_2 films over the past decade. Among them, introducing doping elements, such as W, Mo, Ti, and Mg, is a common approach due to the ability to shift the fermi level in semiconducting VO_2.[17–19] However, increasing the doping level in VO_2 films generally leads to either a reduction in the magnitude of the transition or a broadening of the transition width. Another approach to tune the T_C of VO_2 films is to use epitaxial strain. Muraoka et al reported that the T_C for epitaxial VO_2 films grown on TiO_2 (001) substrates was reduced to 26 °C, while the T_C increased up to 96 °C for VO_2 films grown on TiO_2 (110) substrates.[20] In this case, the correlation between the c-axis length and the T_C showed a reduced T_C by compressing the c-axis. Additionally, various buffer layers have been used between VO_2 films and substrates in order to control the strain and the SMT properties of the VO_2 films including TiO_2,[21] NiO,[22] and Al-doped ZnO.[23] In general, the strain effect of VO_2 films is strongly dependent on the buffer materials and/or substrates used, thus resulting in different

[a]Author to whom correspondence should be addressed. Electronic mail: Heungsoo.kim@nrl.navy.mil.

 © Author(s) 2017

SMT behaviors. SnO_2 functions as an excellent buffer because it has the same tetragonal crystal structure and space group as metallic VO_2 (P42/mnm). Furthermore, due to a close match in lattice constant between SnO_2 ($a = 4.74$ Å, $c = 3.19$ Å, JCPDS #41-1445) and VO_2 ($a = b = 4.54$ Å, $c = 2.88$ Å, JCPDS #71-4821), the VO_2 (001) film can experience in-plane epitaxial strain when deposited on relaxed SnO_2 (001).

Although the structural phase transition from monoclinic (M) phase to tetragonal (T) phase has been observed in VO_2/Al_2O_3 films, recent reports on epitaxially strained VO_2 films grown on lattice matched TiO_2 (001) substrates suggest that no monoclinic phase exists in either insulating and metallic states of ultrathin films.[24,25] Instead, the strained ultrathin VO_2 films undergo a tetragonal-like (T-like) to tetragonal (T) structural transition during the SMT process[26] and exhibit an ultrafast phase transition, which could be used for fast switching optoelectronic applications.[27] However, ultrathin VO_2 films are difficult to produce because it could be easily oxidized to V_2O_5 during device processing, which limits further applications.[28]

In this work, we demonstrate a route for synthesizing thick (50 - 100 nm), partially strained VO_2 films using SnO_2 buffer layers. By depositing (001) oriented SnO_2 buffer layers on m-cut sapphire substrates at various oxygen pressures, we were able to control the interfacial strain of VO_2 films in order to tune the T_C without diminishing the magnitude or sharpness of the transition. Interestingly, x-ray diffraction data shows that the VO_2 films on SnO_2 also exhibit a structural phase transition from T-like VO_2 to T-VO_2 during the SMT process, making these films easier to grow and thus more practical for application based purposes.

II. EXPERIMENTAL METHODS

Epitaxial VO_2/SnO_2 thin film heterostructures were deposited on single crystal (100) Al_2O_3 substrates via pulsed laser deposition (PLD) using a KrF excimer laser (LPX 300, 248 nm, pulse duration of 30 ns). The SnO_2 target was prepared from SnO_2 powder (purity 99.99%, Aldrich) by pressing into 2.54 cm diameter at 10,000 kg and then sintering at 1200 °C for 24h in flowing O_2 atmosphere. A stoichiometric VO_2 target (ACI Alloys) was used for the VO_2 film growth. The chamber was evacuated to a background pressure of $\sim 1 \times 10^{-5}$ Torr, prior to deposition. The SnO_2 buffer layers (~150 nm) were deposited at 550 °C and at oxygen pressures between 10 mTorr and 100 mTorr, followed by VO_2 layers (50-100 nm) grown at 550 °C and a fixed oxygen pressure of 10 mTorr. The electrical switching properties of the VO_2 films were characterized at temperatures between 20 and 100°C. X-ray diffraction (XRD) [Rigaku rotating anode X-ray generator with Cu Kα radiation] was used to characterize the crystal structure of the films.

III. RESULTS AND DISCUSSION

Figure 1a shows the θ-2θ XRD scans of the VO_2/SnO_2 heterostructures as a function of oxygen pressure (10, 30, 100mTorr) during the SnO_2 growth. It can be seen that the strong peak at 68.2° is from the (300) Al_2O_3 substrate [JCPDS #43-1484] whereas the diffraction peak at ~57.8° is assigned to rutile SnO_2 (002), and the diffraction peak at ~65° can be assigned to T-VO_2 (002) reflection, where the red and black dashed lines indicate bulk values for SnO_2 and VO_2, respectively. As the oxygen deposition pressure for SnO_2 film growth decreases, the (002) SnO_2 peak shifts toward lower 2θ angles, while the (002) VO_2 peak shifts toward higher 2θ angles. This XRD result clearly indicates that the out-of-plane lattice constant of SnO_2 films increases and the out-of-plane lattice constant of VO_2 films decreases as the oxygen deposition pressure decreases. This peak shift indicates a different strain state in the VO_2/SnO_2 heterostructure that modifies the SMT properties of VO_2 films.

Epitaxial strain is also influenced by the thickness of VO_2 films. Figure 1(b) shows the θ-2θ XRD scans of VO_2/SnO_2 films with varying VO_2 thicknesses. The VO_2 peak slightly shifts towards lower 2θ angle as the film thickness increases from 50 nm to 100 nm, indicating that the out-of-plane lattice constant of the VO_2 films increases as the film thickness increases. Figure 1c shows the

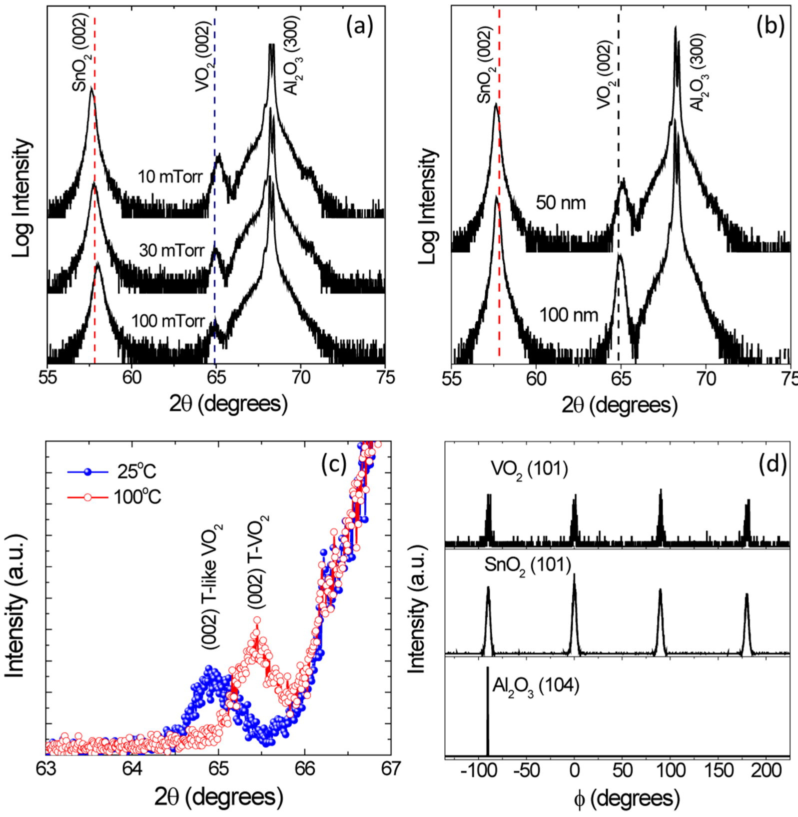

FIG. 1. (a) θ-2θ XRD scans of VO_2/SnO_2 thin films (~50 nm) grown on m-cut sapphire substrates, where the SnO_2 buffer layers were grown at various oxygen pressures (10-100 mTorr). (b) θ-2θ XRD scans of VO_2 films with two different thicknesses (50 and 100 nm) grown on 10 mTorr SnO_2/Al_2O_3 buffer layers. The red broken line represents the bulk SnO_2 (002) peak position and the blue broken line represents the bulk VO_2 (002) peak position in (a) and (b). (c) Temperature-dependent θ-2θ XRD scans of VO_2 film on 30 mTorr SnO_2/Al_2O_3 buffer layer at 25 °C and 100 °C. (d) XRD ϕ-scans of VO_2 (101), SnO_2 (101) and Al_2O_3 (104) peaks of the typical $VO_2/SnO_2/Al_2O_3$ heterostructure.

in-situ temperature-dependent θ-2θ XRD scans of 50 nm-thick VO_2 film on 30 mTorr SnO_2/Al_2O_3 buffer layer measured at 25 °C (semiconducting state) and 100 °C (metallic state). The diffraction peaks can be indexed to the tetragonal (002) VO_2 plane. It is clear that the peak shifts from ~65° to ~65.5° upon the SMT process. The out-of-plane lattice constant calculated from Fig. 1c changes from 2.869 to 2.850 Å with increasing the sample temperature from 25 °C to 100 °C, indicative of a structural transition upon the SMT process. For comparison, it is worth noting that the c-lattice constant does not change upon the SMT process for completely strained 10 nm VO_2 films grown on TiO_2 substrates, thus indicating that no structural phase transition takes place during the SMT process.[24]

In order to verify the epitaxial growth and crystallographic alignment in this heterostructure, XRD ϕ-scans (Figure 1d) were performed on VO_2 (101), SnO_2 (101) and Al_2O_3 (104). As expected the Al_2O_3 exhibits only a single azimuthal peak due to trigonal symmetry. The ϕ-scan of SnO_2 (101) shows four peaks with a rotation of 90° between each peak, indicating fourfold symmetry about the c-axis. One of these peaks has the same ϕ angle with the Al_2O_3 (104) substrate peak, verifying the epitaxial relationship between the SnO_2 buffer layer and the Al_2O_3 substrate. The ϕ-scan of the VO_2 (101) also shows four (101) peaks (T-VO_2), which appear at the same azimuth angles of the SnO_2 (101) peaks, thus verifying the epitaxial growth on the SnO_2 buffer layer. Therefore, 50 nm thick VO_2 film grows epitaxially on the tetragonal SnO_2 buffer layer, and clearly has a similar tetragonal like structure at room temperature. Based on these ϕ-scan results, the in-plane orientation relationship of $VO_2/SnO_2/Al_2O_3$

heterostructure can be deduced as (001)VO_2||(001)SnO_2||(100)Al_2O_3 and [100]VO_2||[100]SnO_2||010] Al_2O_3.

Electrical properties were measured as a function of SnO_2 oxygen growth pressure (10–100 mTorr) (Figure 2a) and as a function of VO_2 thickness (Figure 2b), respectively. It is clear from Figure 2 that all VO_2 films grown on SnO_2 buffer layers show reduced T_C compared to the VO_2 film without the SnO_2 buffer layer. T_C gradually decreases with the reduction of oxygen deposition pressure for SnO_2 buffer layers. This reduction in T_C from 63 °C to 52 °C, for the 100 mTorr and 10 mTorr SnO_2 buffer respectively, can be interpreted as a difference in epitaxial strain between the two films. Generally, VO_2 films having the highest tensile epitaxial strain would exhibit the lowest T_C.[26] Therefore, 10 mTorr appears to be the ideal oxygen deposition pressure for the SnO_2 buffer layer to effectively induce epitaxial strain in VO_2 films. The VO_2 films grown on the 30 mTorr and 100 mTorr SnO_2 layers show slightly higher T_C, suggesting that these films might be slightly more relaxed than the VO_2 film on the 10 mTorr SnO_2 layer. Figure 2c compares the electrical properties of a 50 nm VO_2 film on SnO_2/Al_2O_3 buffer to a 50 nm VO_2 film grown directly on Al_2O_3 substrate. Without the SnO_2 buffer layer, the film is fully relaxed and the T_C is increased to 68 °C close to the bulk VO_2 value.

The thickness-dependent SMT properties were also characterized by measuring the electrical resistivity of the films. As seen in Figure 2b, as the thickness of VO_2 films increases, the magnitude of the SMT increases. However, the T_C of VO_2 films also increases with increasing film thickness because the interfacial strain between the VO_2 film and SnO_2 buffer is expected to relax by misfit dislocations. Additionally, there is a slight reduction in the magnitude of the transition associated with the interfacial strain. Where the 100 nm and 50 nm thick VO_2 films exhibit a 4.5 and 3.5 orders of magnitude change in resistivity, respectively. This again suggests a higher tensile epitaxial strain in the thinner films. Transition temperatures during heating and cooling processes are listed in TABLE I.

Reciprocal space mapping (RSM) measurements were performed to directly determine the interfacial strain and the corresponding lattice constants for epitaxial VO_2 films grown on SnO_2 buffer layers. Figure 3a–c show RSM data for 50 nm thick VO_2 films grown on SnO_2 buffer layers in which the SnO_2 layers were deposited at various oxygen pressures (10, 30, 100 mTorr). The RSM data for a

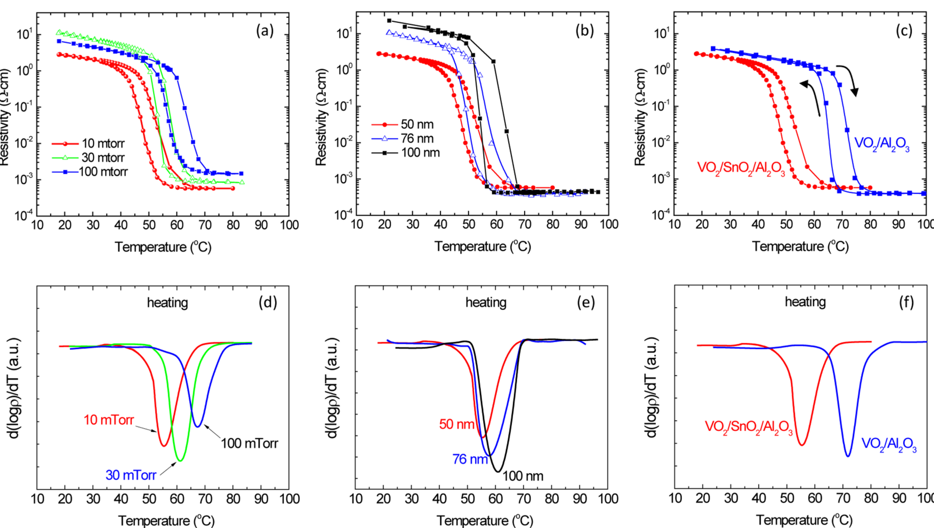

FIG. 2. (a) Electrical resistivity vs temperature for $VO_2/SnO_2/Al_2O_3$ heterostructures, where SnO_2 buffer layers were deposited at various oxygen pressures (10, 30 and 100 mTorr). (b) Electrical resistivity vs temperature for $VO_2/SnO_2/Al_2O_3$ heterostructures with different VO_2 thicknesses (50, 76 and 100 nm). SnO_2 buffer layers for these films were grown at 10 mTorr of oxygen. (c) Electrical resistivity vs temperature for 50 nm VO_2 film on SnO_2/Al_2O_3 (red) and 50 nm VO_2 film on Al_2O_3 (blue), where arrows indicate measurement direction. (d) - (f) Corresponding differential curves of plots in (a), (b) and (c), respectively.

TABLE I. Transition temperatures during heating and cooling processes in Fig. 2 (a–c). $T_{heating}$ and $T_{cooling}$ are the transition temperatures defined as the center of the derivative curves during heating and cooling, respectively. T_{SMT} is defined as the difference between $T_{heating}$ and $T_{cooling}$.

Transition temperature	Oxygen deposition pressure during SnO_2 growth			VO_2 film thickness			VO_2 on m-Al_2O_3 with/without 10 mTorr SnO_2 buffer	
	10 mTorr	30 mTorr	100 mTorr	50 nm	76 nm	100 nm	With SnO_2	Without SnO_2
$T_{heating}$ (°C)	55.6	61.2	66.9	55.6	61.9	62.4	55.6	72.8
$T_{Cooling}$ (°C)	48.4	56.6	59.6	48.4	51.5	54.0	48.4	64.2
T_{SMT} (°C)	52.0	58.9	63.2	52.0	56.7	58.2	52.0	68.5

100 nm VO_2 film on 10 mTorr SnO_2 buffer is also provided (Figure 3d). RSMs were performed about the (112) diffraction peak for rutile SnO_2. The bulk Qx and Qz values for SnO_2 and T-VO_2 are marked in each panel with a triangle symbol and a square symbol, respectively. For the VO_2 film grown on 10 mTorr SnO_2 buffer layer (Figure 3a), the Qz value for VO_2 peak is observed to be slightly larger than the bulk Qz value of T-VO_2, indicating that the film shows out-of-plane compressive strain. Furthermore, the Qx value for VO_2 peak mainly falls between the Qx of SnO_2 and the square symbol, indicating that the film is partially strained to the SnO_2 buffer layer with in-plane tensile strain. For the VO_2 film on 100 mTorr SnO_2 buffer layer (Figure 3c), the Qx and Qz values of the VO_2 peak are observed to be much closer to the bulk VO_2 (square symbol) than the films grown on 10 and 30 mTorr (Figures 3a,b) SnO_2 buffer layers. This shift of the Qx and Qz values indicates that the film on 100 mTorr SnO_2 buffer is more relaxed than the films grown on 10 and 30 mTorr SnO_2 buffers but still exhibiting a partially strained state. The reason that more strain is introduced in the VO_2 films

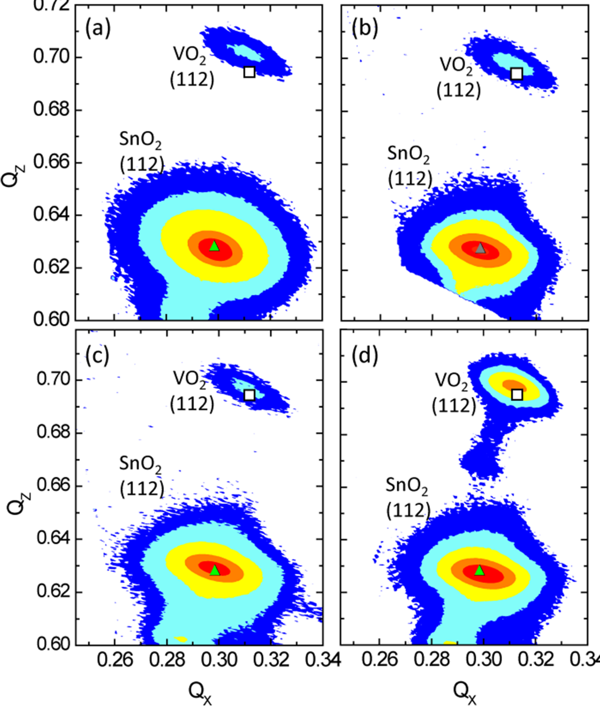

FIG. 3. RSMs of VO_2 films (50 nm) deposited on SnO_2 buffer layers, where SnO_2 layers were grown at various oxygen pressures of (a) 10 mTorr, (b) 30 mTorr and (c) 100 mTorr. (d) RSM of 100 nm VO_2 film deposited on 10 mTorr-SnO_2 buffer layer. All scans are about the (112) diffraction spot of SnO_2. The square marks represent the expected Qx and Qz values for bulk T-VO_2 (112) and the triangle symbols represent the bulk SnO_2 (112) spot.

grown on 10 and 30 mTorr SnO_2 buffers is related to increased *c*-axis of SnO_2 buffer (compared to 100 mTorr SnO_2), which leads to decreased *a*-axis of SnO_2 buffer. Thus, decreasing SnO_2 oxygen deposition pressure would lower the in-plane lattice mismatch between the VO_2 film and SnO_2 buffer, which helps to sustain more epitaxial strain in the VO_2 film. Furthermore, no M-VO_2 peaks were observed in (112) RSMs, verifying again that the VO_2 films on SnO_2/Al_2O_3 buffer layers at room temperature is a T-like phase. Similar results have been reported on VO_2 films grown on TiO_2 substrate by other groups.[26]

Since the in-plane lattice constant of VO_2 (a=0.455 nm) is smaller than that of SnO_2 (a=0.474 nm), the c-axis lattice constant of VO_2 films epitaxially grown on SnO_2 should decrease due to an in-plane tensile stress at the interface (lattice mismatch: 4.0%). In general, increasing in-plane tensile strain (i.e., compressive out-of-plane strain) leads to a reduced T_C in epitaxial VO_2 films.[19,21] Figure 4 shows the values of *c*/*a* for VO_2 films as a function of SnO_2 growth pressure and thickness of VO_2 films. The *a*- and *c*-axis lattice constants of VO_2 films were determined by analyzing the proportional relation between the spots of VO_2 and SnO_2 in RSM data. It is clear that the value of *c*/*a* ratio decreases as the SnO_2 growth pressure decreases (Figure 4a) or the VO_2 film thickness decreases (Figure 4b), and reducing the *c*/*a* ratio for VO_2 films can lead to a reduced T_C. Our results are similar to the previous reports on VO_2 films grown on TiO_2 (001) or MgF_2 substrates.[20,29] According to the Clausius-Clapeyron equation,[30] increasing the in-plane tensile strain of T-VO_2 leads to a decrease in T_C. Our RSM results clearly indicate that tensile strain increases along the a-axis while compressive strain increases along the c-axis of the VO_2 lattice, thus leading to the decrease in T_C. It is worth noting that the thicker VO_2 film (100 nm) still shows a lower T_C (~58 °C)

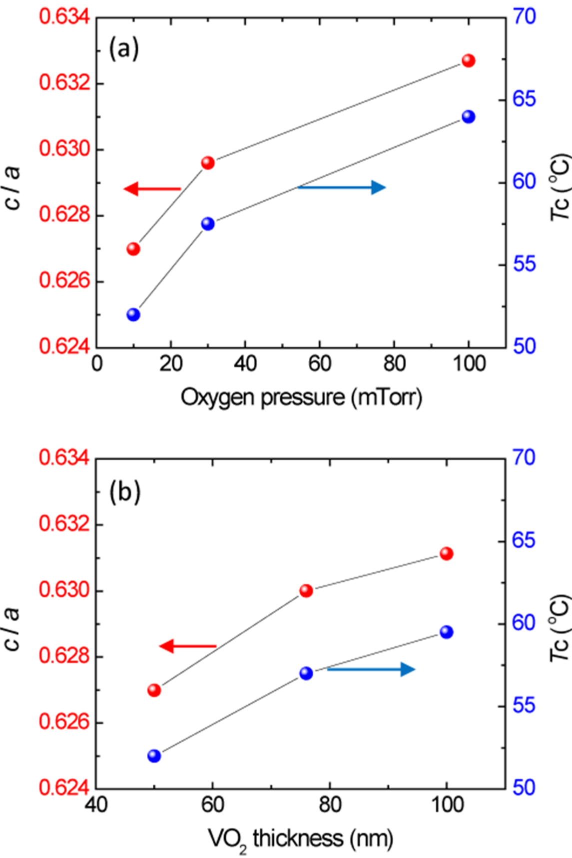

FIG. 4. (a) The c/a ratio and transition temperature (T_C) for 50 nm VO_2 films deposited on SnO_2 buffer layers, where SnO_2 layers were grown at various oxygen pressures (10, 30, 100 mTorr). (b) The c/a ratio and T_C as a function of VO_2 film thicknesses (50, 76, 100 nm) for VO_2 films grown on 10 mTorr SnO_2 buffer layers.

compared to that of bulk VO_2 (~68 °C) most likely due to residual strain caused by the SnO_2 buffer layer.

IV. CONCLUSIONS

In summary, we report the ability to synthesize thick (50-100 nm), partially strained VO_2 films exhibiting reduced Tc's down to 52 °C by growing VO_2/SnO_2 heterostructures epitaxially onto m-cut Al_2O_3 substrates. By adjusting the O_2 pressure during SnO_2 growth, we are able to control the interfacial strain between the VO_2 films and SnO_2 buffer layer and, accordingly, tune the T_C (52-68 °C) of the VO_2 films without diminishing the magnitude or sharpness of their transition. Furthermore, the resulting heterostructures suppress the monoclinic-VO_2 phase, giving rise to a tetragonal-like to tetragonal structure transition during the SMT process. Our results establish a practical route for synthesizing VO_2 films with tunable SMT properties and provide an important step towards their practical implementation.

ACKNOWLEDGMENTS

This work was funded by the Office of Naval Research (ONR) through the Naval Research Laboratory Basic Research Program.

[1] F. J. Morin, Phys. Rev. Lett. **3**, 34 (1959).
[2] M. F. Becker, A. B. Buckman, R. M. Walser, T. Lepine, P. Georges, and A. Burn, Appl. Phys. Lett. **65**, 1507 (1994).
[3] H.-T. Kim, B.-J. Kim, S. Choi, B.-G. Chae, Y. W. Lee, T. Driscoll, M. M. Qazilbash, and D. N. Basov, J. Appl. Phys. **107**, 023702 (2010).
[4] A. Cavalleri, C. Tóth, C. Siders, J. Squier, F. Ráksi, P. Forget, and J. Kieffer, Phys. Rev. Lett. **87**, 237401 (2001).
[5] A. Cavalleri, Th. Dekorsy, H. H. W. Chong, J. C. Kieffer, and R. W. Schoenlein, Phys. Rev. B **70**, 161102 (2004).
[6] M. Nakano, K. Shibuya, D. Okuyama, T. Hatano, S. Ono, M. Kawasaki, Y. Iwasa, and Y. Tokura, Nature **487**, 459 (2012).
[7] Y. Zhou and S. Ramanathan, J. Appl. Phys. **111**, 084508 (2012).
[8] N. A. Charipar, H. Kim, S. A. Mathews, and A. Piqué, AIP Advances **6**, 015113 (2016).
[9] A. Pashkin, C. Küber, H. Ehrke, R. Lopez, A. Halabica, R. F. Haglund, R. Huber, and A. Leitenstorfer, Phys. Rev. B **83**, 195120 (2011).
[10] T. Driscoll, H.-T. Kim, B.-G. Chae, M. Di Ventra, and D. N. Basov, Appl. Phys. Lett. **95**, 043503 (2009).
[11] H. Kim, N. Charipar, M. Osofsky, S. B. Qadri, and A. Piqué, Appl. Phys. Lett. **104**, 081913 (2014).
[12] L. Wang, E. Radue, S. Kittiwatanakul, C. Clavero, J. Lu, S. A. Wolf, I. Novikova, and R. A. Lukaszew, Opt. Lett. **37**, 4335 (2012).
[13] H. Kim, N. Charipar, E. Breckenfeld, A. Rosenberg, and A. Piqué, Thin Solid Films **596**, 45 (2015).
[14] D. Porwal, A. C. M. Esther, I. N. Reddy, N. Sridhara, N. P. Yadav, D. Rangappa, P. Bera, C. Anandan, A. K. Sharma, and A. Dey, RSC Adv. **5**, 35737 (2015).
[15] J. B. Cao, W. Fan, Q. Zhou, E. Sheu, A. W. Liu, C. Barrett, and J. Wu, J. Appl. Phys. **108**, 083538 (2010).
[16] B. J. Kim, Y. W. Lee, B. G. Chae, S. J. Yun, S. Y. Oh, H. T. Kim, and Y. S. Lim, Appl. Phys. Lett. **90**, 023515 (2007).
[17] X. Tan, T. Yao, R. Long, Z. H. Sun, Y. J. Feng, H. Cheng, X. Yuan, W. Q. Zhang, Q. H. Liu, C. Z. Wu, Y. Xie, and S. Q. Wei, Sci. Rep. **2**, 466 (2012).
[18] N. R. Mlyuka, G. A. Niklasson, and C. G. Granqvist, Appl. Phys. Lett. **95**, 171909 (2009).
[19] K. L. Holman, T. M. McQueen, A. J. Williams, T. Klimczuk, P. W. Stephens, H. W. Zandbergen, Q. Xu, F. Ronnig, and R. J. Cava, Phys. Rev. B **79**, 245114 (2009).
[20] Y. Muraoka and Z. Hiroi, Appl. Phys. Lett. **80**, 583–5 (2002).
[21] E. Breckenfeld, H. Kim, K. Burgess, N. Charipar, S.-F. Cheng, R. Stroud, and A. Piqué, ACS Appl. Mater. Interfaces **9**, 1577–1584 (2017).
[22] A. Gupta, J. Narayan, and T. Dutta, Appl. Phys. Lett. **97**, 151912 (2010).
[23] J. Jian, X. Wang, L. Li, M. Fan, W. Zhang, J. Huang, Z. Qi, and H. Wang, ACS Appl. Mater. Interfaces **9**, 5319–5327 (2017).
[24] M. Yang, Y. Yang, B. Hong, L. Wang, K. Hu, Y. Dong, H. Xu, H. Huang, J. Zhao, H. Chen, L. Song, H. Ju, J. Zhu, J. Bao, X. Li, Y. Gu, T. Yang, X. Gao, Z. Luo, and C. Gao, Sci. Rep. **15**, 23119 (2016).
[25] L. L. Fan, S. Chen, Z. L. Luo, Q. H. Liu, Y. F. Wu, L. Song, D. X. Ji, P. Wang, W. S. Chu, C. Gao, C. W. Zou, and Z. Y. Wu, Nano Lett. **14**, 4036–4043 (2014).
[26] H. Qiu, M. Yang, Y. Dong, H. Xu, B. Hong, Y. Gu, Y. Yang, C. Zou, Z. Luo, and C. Gao, New J. Phys. **17**, 113016 (2015).
[27] R. J. Suess, N. S. Bingham, K. M. Charipar, H. Kim, S. A. Mathews, A. Piqué, and N. A. Charipar, Adv. Mater. Interfaces 1700810 (2017).
[28] Y.-X. Ji, S.-Y. Li, G. A. Niklasson, and C. G. Granqvist, Thin Solid Films **562**, 568 (2014).
[29] L. L. Fan, S. Chen, G. M. Liao, Y. L. Chen, H. Ren, and C. W. Zou, J. Phys.: Condens. Matter **28**, 255002 (2016).
[30] J. Cao, E. Ertekin, V. Srinivasan, W. Fan, S. Huang, H. Zheng, J. W. L. Yim, D. R. Khanal, D. F. Ogletree, J. C. Grossman, and J. Wu, Nature Nanotechnology **4**, 732–737 (2009).